Indian Journal of Pure & Applied Physics
Vol. 60, June 2022, pp. 509-520

Photocatalytic Study of Mo/N co-doped Titanium Dioxide (TiO_2) Nanoparticles Under Visible Light Irradiation

Anju Rani[a], Suresh Kumar[a], R L Dhiman[b]*, Virender Singh[c] & Suresh Kumar[c]

[a]Department of Physics, M.M. (Deemed to be University), Mullana-Ambala, Haryana-133 207, India

[b]Department of Physics, Sanatan Dharma College (Lahore), Ambala Cantt.-133 001, India

[c]Department of Electronics Science, Kurukshetra University, Kurukshetra-136 119, India

Received 3 March 2022; accepted 6 May 2022

Undoped TiO_2 and Mo/N co-doped TiO_2 nanoparticles have been fabricated by sol gel technique. The average particle size of nanoparticles was calculated from the line broadening of (101) peak of XRD pattern and further verified by High Resolution Transmission Electron Microscopy (HRTEM) are in good agreement. The decrease in particle size 28.5 to 15.0 nm was observed with increase of molybdenum concentration. The surface morphology of all samples was studied by Field Emission Scanning Electron Microscopy shows small agglomeration. The optical band gap energy was calculated using UV-visible absorption spectroscopy and found to decrease in increase of doping concentration. The presence of defect levels caused by oxygen vacancies has been confirmed by Photoluminescence spectra. The emission bands observed at 453.9, 470.6, 485.7, 495.8 and 535 nm could be arising from surface states. The phase composition and elemental analysis of synthesized samples was estimated from Energy dispersive X-ray spectroscopy. The effect of doping concentration on structural formation was studied by FTIR spectroscopy. The Photocatalytic activity of synthesized samples for degradation of Congo red (CR) and Methyl orange (MO) dyes as standard pollutants was investigated under visible light source. The increase in doping concentration causes enhance in photocatalytic activity of the synthesized nanoparticles which is attributed from the decrease in electron-hole pair recombination rates. The degradation efficiency against congo red dye is very high compared to methyl orange dye. These observations suggest that co-doped synthesized nanoparticles are suitable for complete degradation of congo red dye and are not able to degrade methyl orange dye.

Keywords: Nanoparticles; codoped TiO_2; Photocatalytic degradation of organic dyes

1 Introduction

World is facing environmental problems due to modernization in industrial growth that causes air and water pollution at large extant in form of waste from different industries[1]. As for as lather and textile industries are concerned heavy metals and dyes discharged through waste water are the main sources of water pollution[2-3]. Therefore the main challenge before the scientific community is how to reduce the water pollution. Traditional processes such as combined coagulation, electrochemical oxidation, active sludge, flocculation, reverse osmosis and adsorption on activated carbon have recently been investigated and proved to be adequate. But these methods are not effective to purify highly contaminated water due to production of more concentrated pollutant containing phase in waste water[4]. Photocatalysis is eco-friendly and suitable technique which offers great potential for the complete elimination of toxic chemicals from the environment through its efficiency and broad applicability[5]. Photocatalysis is a promising green technology in which solar energy is converted into chemical energy for degradation of organic pollutants into harmless inorganic substances such as CO_2 and H_2O[6]. Metal oxide nanostructures, such as TiO_2, ZnO, CeO_2, and SnO_2, semiconductors have attracted considerable interest for being used as a photocatalyst due to their great potential in the photocatalytic oxidation of organic pollutants[7]. Among these semiconductors, TiO_2 has been considered as the most promising Photocatalyst owing to its excellent properties such as low cost, non-toxicity, high stability, biological and chemical inertness, high refractive index, low absorption coefficient and high oxidation power[8]. However, the degradation efficiency of TiO_2 photocatalytic is restricted limited due to its wide band gap (3.2 eV) can only be activated under 3-5% UV light of total solar

*Corresponding author:
(E-mail: roshandhiman_kuk@yahoo.co.in)

spectrum[9-10] and other due to high recombination rate of photo generated charge carriers[7]. To overcome these problems considerable efforts has been made by scientific community. During the past decade sufficient work related to doping of single metal/non-metal in TiO_2 for degradation of organic pollutants has been reported[11-15]. Furthermore, it has been well established that the co-doped TiO_2 with both metal/non-metal simultaneously could reduce the charge carries recombination rate enhanced photocatalytic degradation efficiency significantly[16-21]. Doping of nitrogen atoms have attracted the most attention because of its comparable atomic size with oxygen, small ionization energy, metastable center formation, high stability, low cost and significant enhancement of photocatalytic activity under visible light[22]. It has been reported that co-doping of Mo & N in TiO_2 nanoparticles enhance higher photocatalytic activity for degradation of organic dyes under visible light compared to Mo doping[23-27]. In the present report sol-gel method has been employed to synthesize Mo/N co-doped TiO_2 with different Mo doping concentration. The structural, optical, and morphological studies were carried out using various techniques such as X-Ray diffraction, UV-visible absorption spectroscopy, Photoluminescence, Fourier transform infrared spectroscopy, Field emission scanning electron microscopy with energy dispersive X-ray spectroscopy and High resolution transmission electron microscopy. The photocatalytic activities of the synthesized nanoparticles were studied over Congo red and Methyl orange dye under visible light irradiation.

2 Experimental details

2.1 Materials

For synthesis of nanoparticles analytical grade chemical reagents were used without further purification; Molybdenum oxide purchased from Himedia, titanium IV isopropoxide (TTIP) and Urea were supplied from Sigma Aldrich. Moreover, Methanol and DI water were used as solvents throughout the experiment.

2.2 Synthesis of Mo/N doped TiO_2 nanoparticles

The undoped TiO_2 and Mo/N co-doped TiO_2; $Ti_{0.95-x}Mo_xN_{0.05}O_2$ (x = 0.04, 0.08 & 0.12 mol %) nanoparticles have been synthesized by sol-gel technique. To prepare 0.04 mol % of codoped TiO_2 nanoparticles, 13 ml of TTIP was diluted with 50 ml of methanol under constant stirring at room temperature and kept in dark. Then 0.29 gm of molybdenum oxide (MoO_3) and 0.15 gm urea dissolved in small amount of warm DI water having 0.8 ml concentrated HNO_3 mixed with TTIP solution under vigorous stirring. The obtained homogeneous solution was magnetically stirred continuously for 5 hours to form a highly viscous sol. The resulting sol was kept under agitation for 3 h then filtered and washed with methanol several times to obtained gel. The gel was dried at 100^oC in hot air oven for 24 hours after grinded in agate mortar then finally annealed at 400 ^oC for 4 hours in muffle furnace to obtain 0.04 mol % Mo/N doped TiO_2 nanoparticles. The stepwise experimental procedure for synthesis of 0.04 mole % Mo/N doped TiO_2 is presented in Fig. 1. Similar procedure is followed for other higher concentrations using appropriate weight amount of materials. Undoped TiO_2 nanoparticles were synthesized using same procedure as followed for co-doped samples.

2.3 Characterization of synthesized nanoparticles

The structural formation of synthesized nanoparticles was investigated through X-ray diffraction measurements carried out at room temperature using Cu-Kα radiation of wavelength 1.5406 Å. The stable phase formation of synthesized samples was further verified from FTIR spectra recorded at room temperature in the spectral range 400-4000 cm^{-1} on Perkin Elmer FTIR spectrophotometer. The optical band gap energy was calculated from absorption spectra recorded at room temperature in the spectral range 200-800 nm using Perkin Elmer UV-visible spectrophotometer. The elemental composition of the prepared samples was estimated from Energy dispersive X-ray spectroscopy attached to SEM. The surface morphology and particle size were determined from SEM and High resolution transmission electron microscopy respectively. The formation of energy sub states within forbidden gap of TiO_2 was verified by Photoluminescence spectra recorded at room temperature in wave length region 400-500 nm. The photocatalytic activity of prepared nanoparticles was investigated against degradation of congo red and methyl orange dye under visible light source of wavelength 400-700 nm.

3 Results and Discussion

3.1 X-ray diffraction analysis

The X-ray diffraction (XRD) was used to investigate the crystal structure and phase formation

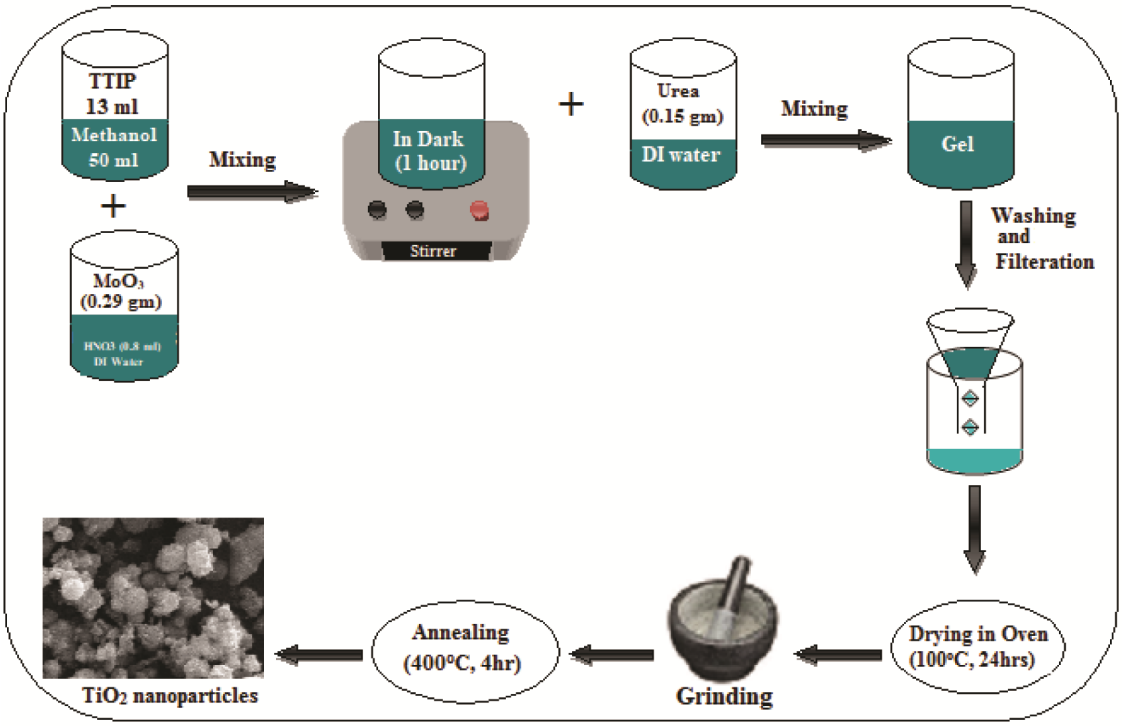

Fig. 1 — Schematic presentation of the synthesis process of codoped $Ti_{0.95-x}Mo_xN_{0.05}O_2$; x = 0.04 mol % nanoparticles.

of synthesized nanoparticles. The diffraction patterns of all synthesized samples were recorded on X-ray diffractometer scanned in the 2θ range of 10°–80° with a step size of 0.02°. The recorded XRD patterns of the synthesized samples are illustrated in Fig. 2. The diffraction peaks appears at angle 25.45°, 38°, 48.16°, 54.07°, 55.21°, 62.89°, 68.90°, 70.46°, 75.13° corresponding to (101), (004), (200), (105), (211), (204), (116), (220), (215) crystal planes of anatase TiO_2 phase were assigned and are in good agreement with standard data file (JCPDS card no. 84-1285). All peaks identified in the as-synthesized samples are completely in accordance with anatase phase of TiO_2 and no peak related to the rutile phase. Due to compareable ionic radii of Mo^{6+} (0.062 nm) with Ti^{4+} (0.068 nm) and N^{3-} (0.013 nm) with O^{2-} (0.014 nm), Mo and N ions are perfectly incorporated into TiO_2 lattice[26]. Moreover, the XRD patterns reveal that the broadening of peak increases with increase in Mo doping concentration is attributed to the decrease in crystallite size due to the replacement of TiO_2 by Mo element[28]. The average crystallite sizes of as synthesized samples were calculated from full width at half-maximum of the most intense (101) diffraction peak using Debye-Scherrer equation[29].

$$D = K\lambda/\beta\cos\theta \quad \ldots (1)$$

where D is the average crystallite size in nm, K is a shape factor (0.89), λ is the wavelength of the X-ray radiation (Cu Kα = 0.15406 nm), β is the full width at half maximum (FWHM) of (101) diffraction peak, θ is Bragg's diffraction angle. The calculated average values of crystallite size of synthesized samples are listed in Table 1.

3.2 Field Emission Scanning Electron Microscopy

The surface morphology of undoped and Mo/N co-doped TiO_2 nanoparticles was investigated under field emission scanning electron microscope. The micrograph image Fig. 3(a) of undoped sample shows that the synthesized nanoparticles are somewhat less spherical and more agglomerated. The agglomeration decreases and particles appear more spherical on higher doping concentration as displayed in Fig. 3 (b-c). With increase in Mo doping content results in formation of uniform particles and is due to nucleation effect[30].

3.3 Energy dispersive X-ray spectroscopy analysis

The elemental and phase compositions was analyzed with energy dispersive X-ray spectroscopy (EDXS) and recorded spectra of undoped sample displayed in Fig. 4(a) revealed the presence of Ti and O in peak ratio 1:2 confirm the of formation of stable anatase phase of TiO_2. The EDXS mapping of co-

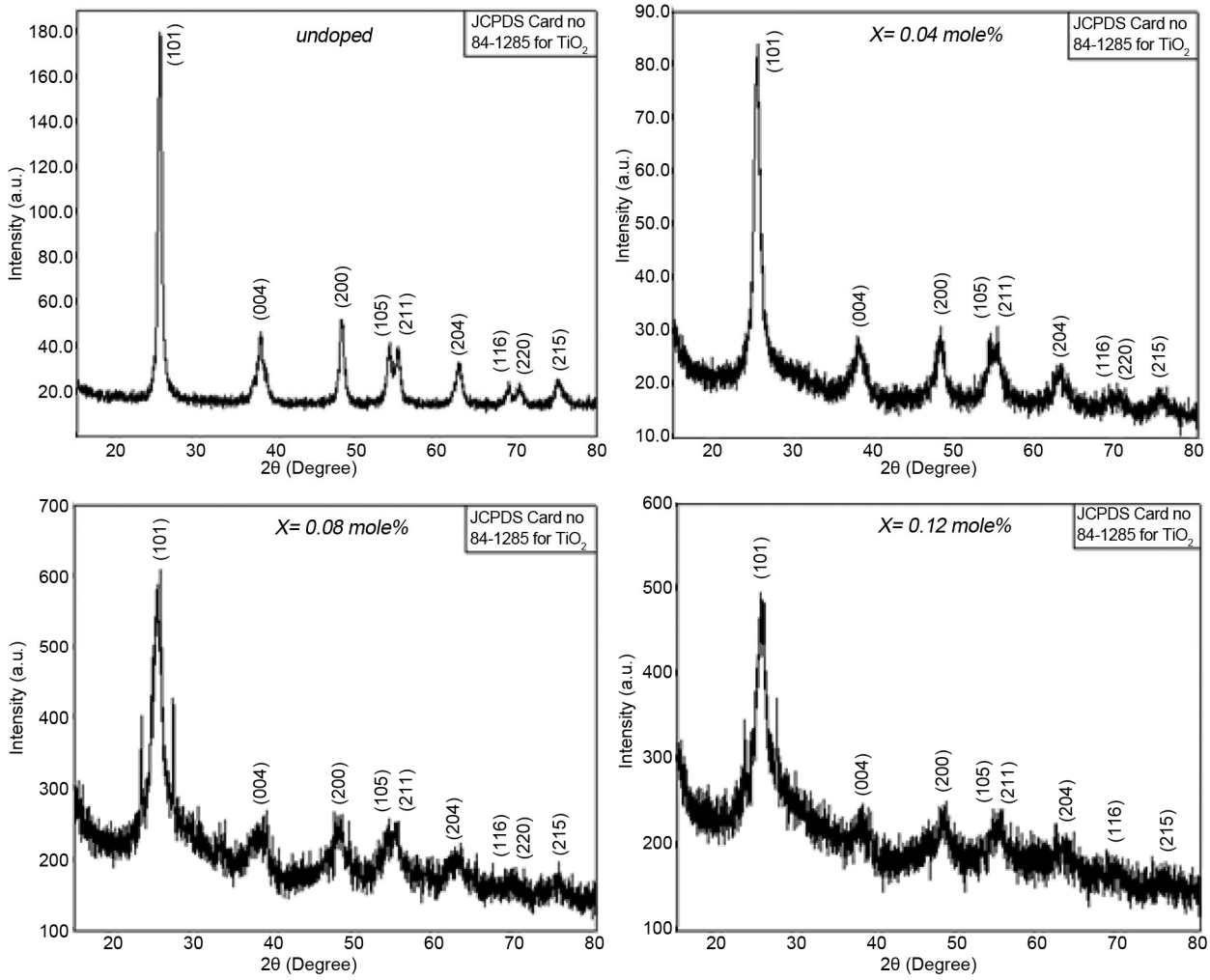

Fig. 2— X-ray diffraction pattern of undoped TiO_2 and codoped $Ti_{0.95-x}Mo_xN_{0.05}O_2$; x = 0.04, 0.08 & 0.12 mol % nanoparticles

Table 1 — X-ray diffraction parameter, crystalline size, band gap energy of undoped and co-doped TiO_2; $Ti_{(0.95-x)}Mo_xN_{0.05}O_2$; x = 0.04, 0.08 & 0.12 nanoparticles.

Sample Matrix ($Ti_{(0.95-x)}Mo_xN_{0.05}O_2$)	Diffraction Angle 2θ (degree)	Crystallite Size (nm) From XRD	Crystallite Size (nm) From TEM	Band gap (Eg) eV
Undoped TiO_2	25.24	28.5	29.0	3.18
x = 0.04 mol%	25.45	20.0	--	2.51
x = 0.08 mol%	25.45	16.2	--	2.18
x = 0.12 mol%	25.24	15.0	14.0	1.59

doped samples Fig. 4 (b-d) confirm that the composites consists of Mo, N, Ti and O elements in appropriate amount . The existence of all elements i.e. Ti, O, Mo and N in the EDXS pattern indicate that TiO_2 nanoparticles have been successfully co-doped with nitrogen and molybdenum.

3.4 HRTEM analysis

TEM was used to study the surface morphology and to verify the particle size of the synthesized nanoparticles estimated from X-ray diffraction. The recorded micrographs of undoped and 0.12 mole% Mo/N doped TiO_2 are displayed in Fig. 5 (a-b). The particle sizes determined from TEM micrographs are in well agreement with XRD measurements.

3.5 Photoluminescence spectroscopy analysis

The photoluminescence spectroscopy (PL) is useful technique to study the separation and recombination of photogenerated electron-hole pairs[31]. Therefore the

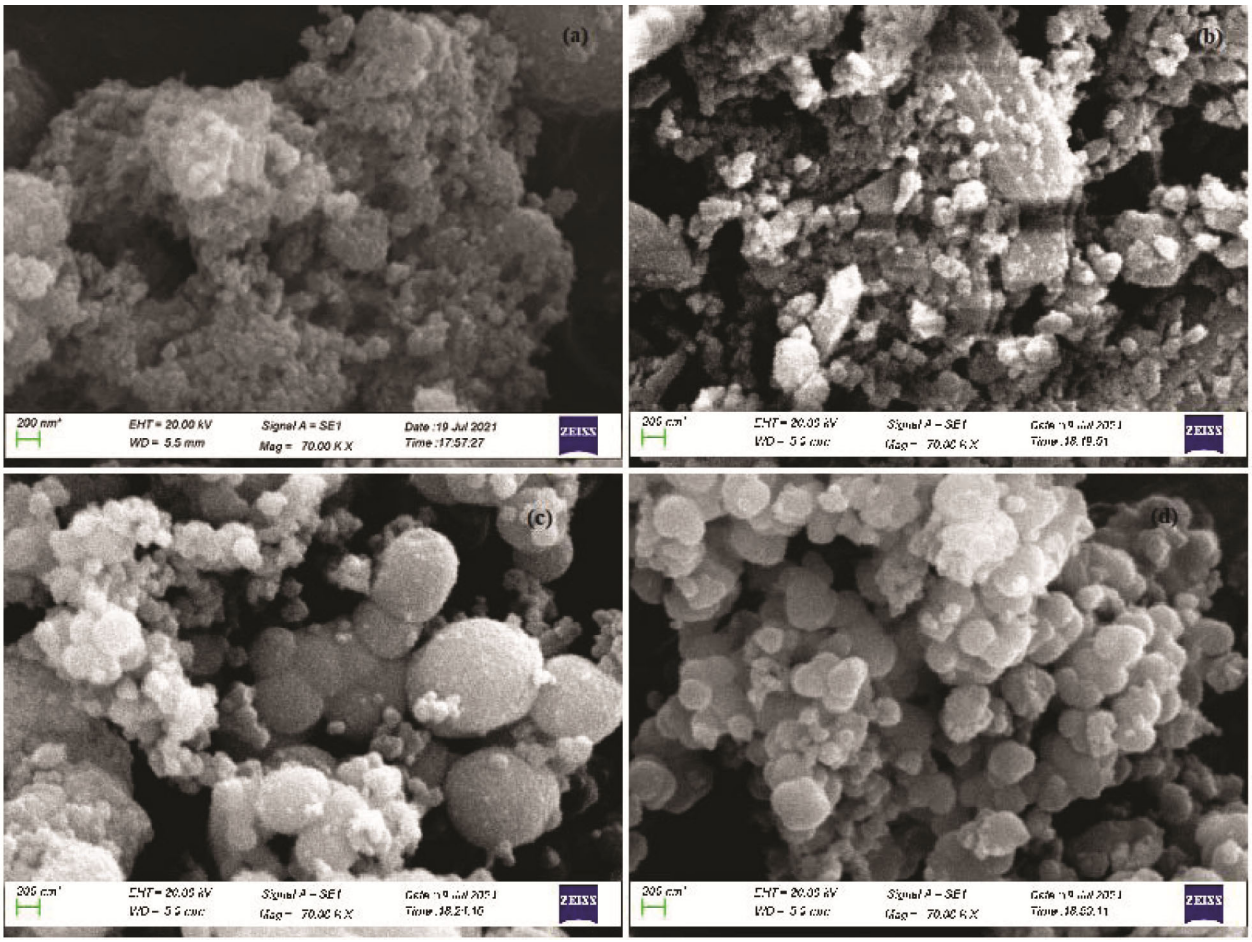

Fig. 3 — FESEM images of (a) undoped TiO_2 nanoparticles (b) co-doped $Ti_{0.95-x}Mo_xN_{0.05}O_2$; x = 0.04 mol % nanoparticles (c) Co-doped $Ti_{0.95-x}Mo_xN_{0.05}O_2$; x = 0.08 mol % nanoparticles (d) co-doped $Ti_{0.95-x}Mo_xN_{0.05}O_2$; x = 0.12 mol % nanoparticles at resolution of 200 nm

synthesized samples were characterized through Photoluminescence spectroscopy at excitations wavelength of 390 nm at room temperature. The recorded PL spectra of synthesized nanoparticles are displayed in Fig. 6. Four well defined peaks appear in the range of 400–500 nm might be originated from the defects levels within the forbidden gap of TiO_2. On increasing dopant concentration the reduction of the intensities of these peaks arises from trapping centers suggest that there is decrease in the carrier recombination rate[32]. The emission peak observed at 485.7 nm can be ascribed to the charge transfer from Ti to O atom in TiO_6 octahedra associated with oxygen vacancies[25]. Broad emissions are observed in the spectral range from 500 to 600 nm. The peaks at 535 nm can be accredited to trapped or bound electrons of oxygen vacancy centers**.** In our samples, it is clear that the PL emission peaks of TiO_2 get quenched by doping and introduce energy states below the CB of TiO_2 which could suppress electron–hole recombination. The concentration of oxygen vacancy centers depends on the concentration of Mo[26]. It is widely accepted that a high concentration of dopant creates electron–hole pairs recombination centers that generates more oxygen vacancies which acts as trapping center[28]. Thus photo generated electrons could be easily trapped in the oxygen vacancies which reduces the probability of electron–hole recombination. The formation of oxygen vacancies depends on the concentration of Mo dopant because with increase in dopant concentration the cleavage of Ti–O bonds increases and there occurs contraction of O–Ti–O bond angle[26]. As PL emission mainly arises from the electron-hole recombination and decrease in intensity of observed spectra suggest the electron-hole pair recombination rate decreases.

3.6 UV-Vis absorption spectroscopy analysis

The optical measurements of prepared samples were carried out using UV-Vis absorption

spectroscopy at room temperature. The recorded absorption spectra are displayed in Fig. 7(a). On increasing doping concentration the absorption edge shifted to higher wavelength region corresponds to red shift indicates the reduction in optical band gap energy[33]. Based on the absorption spectra, the optical band-gap energy was calculated by using Tauc's plot[33]

$$(\alpha h\nu)^{1/n} = B\,(h\nu - E_g) \quad \ldots (2)$$

where α is the optical absorption coefficient, h is the Planck's constant, ν is the frequency of light, B is constant of proportionality, E_g is the band gap energy in eV and n is 2 for indirect band gap semiconductor. Due to indirect band transition of synthesized samples Tauc's plot $[(\alpha h\nu)^{1/2}$ vs $h\nu]$ Fig. 7(b) was used to estimate the band-gap energies by drawing

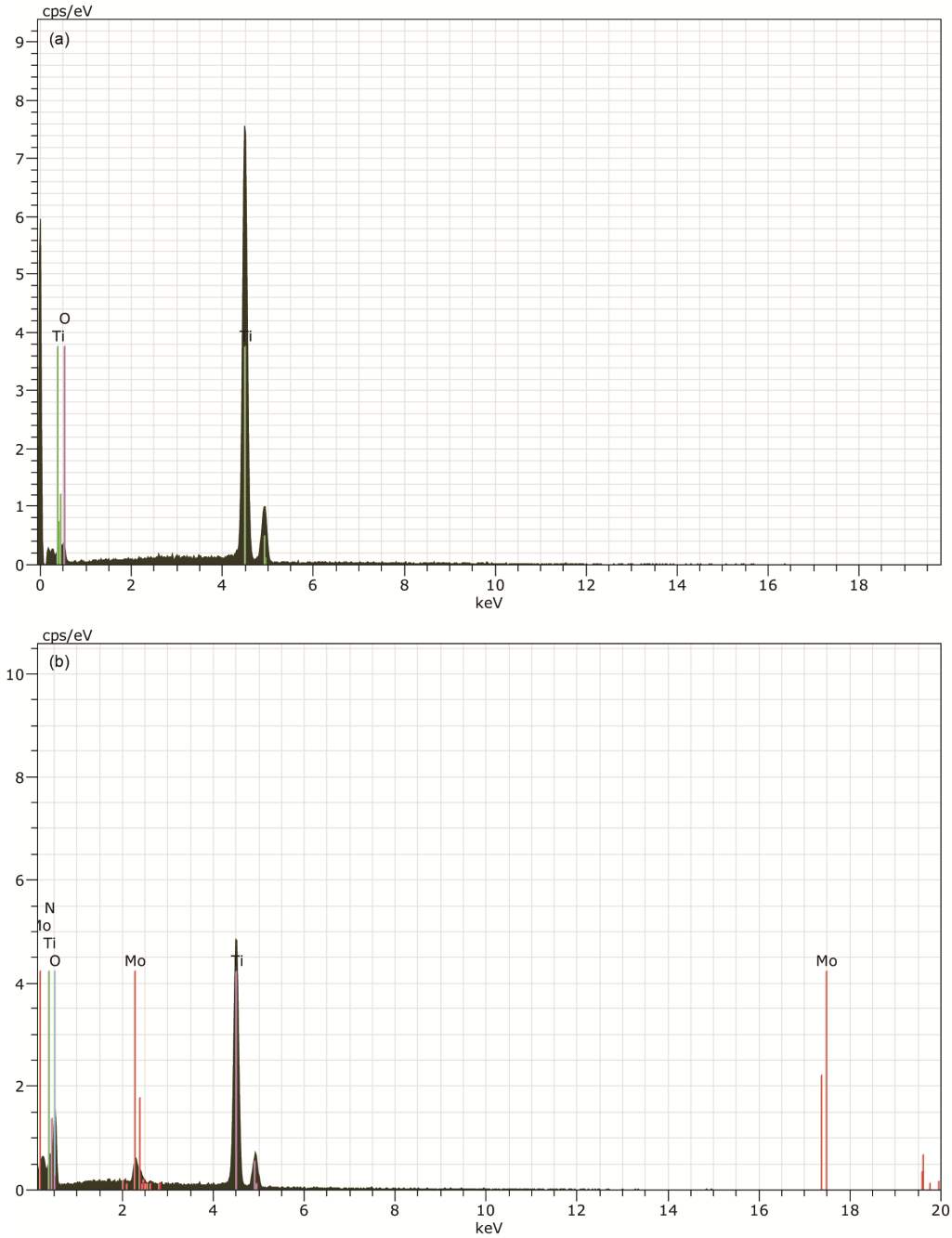

Fig. 4 — (a) EDXS spectra of undoped TiO_2 nanoparticles, (b) EDXS spectra of codoped $Ti_{0.95-x}Mo_xN_{0.05}O_2$; x = 0.04 mole % nanoparticles.

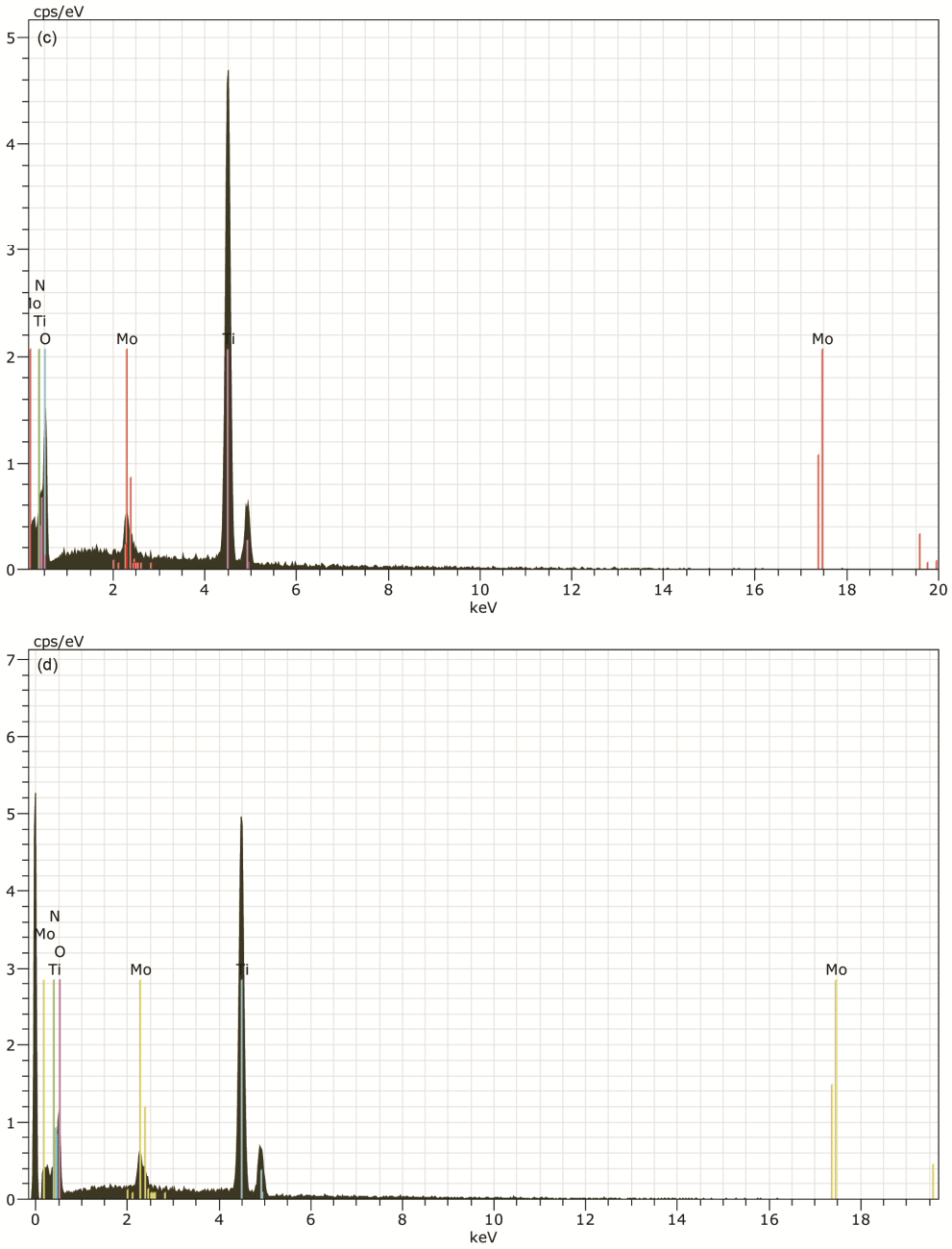

Fig. 4 — (c) EDXS spectra of codoped $Ti_{0.95-x}Mo_xN_{0.05}O_2$; x = 0.08 mol % nanoparticles, (d) EDXS spectra of codoped $Ti_{0.95-x}Mo_xN_{0.05}O_2$; x = 0.12 mol % nanoparticles.

extrapolation of the data point to photon energy axis. The calculated values of band gap energies are listed in Table 1. The observed value of the bandgap energy decreases with the increasing Mo dopant concentration is ascribed to the formation of dopant energy levels within the forbidden gap of TiO_2[34].

3.7 Fourier transforms infrared spectroscopy analysis

The FTIR spectra of the prepared samples recorded in the spectral range 400–4000-cm^{-1} are presented in Fig. 8. Three main absorption peaks appeared at 529.05, 1636.11 and 3347.53 cm^{-1} in each synthesized sample are assigned in observed spectra. The peak observed at 529.05cm^{-1} is assigned to banding vibration of Ti–O bond in anatase TiO_2 lattice[35]. In the present spectra an absorption peak appearing around 1636.11 cm^{-1} confirms the stable anatase phase of TiO_2[14]. The peak observed around 3347.53 cm^{-1} corresponds to the stretching vibrations of O-H group adsorbed onto the surface of the synthesized samples[35].

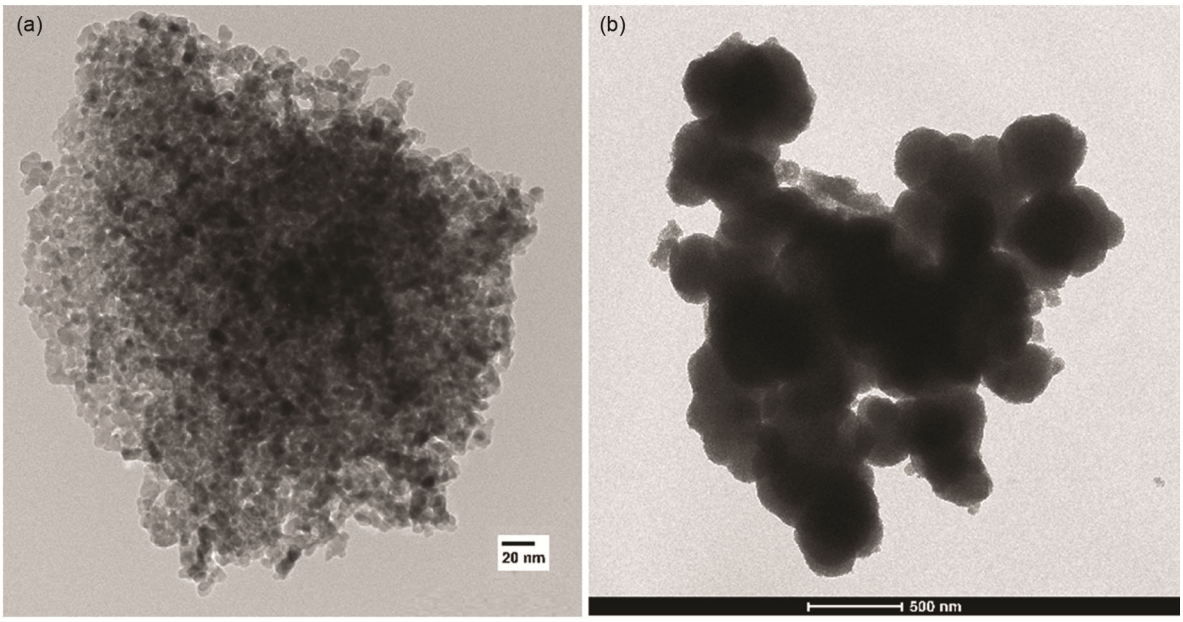

Fig. 5 — HRTEM images of undoped TiO_2 and co-doped $Ti_{0.95-x}Mo_xN_{0.05}O_2$; x = 0.12 mol % nanoparticles at 20 nm and 500 nm.

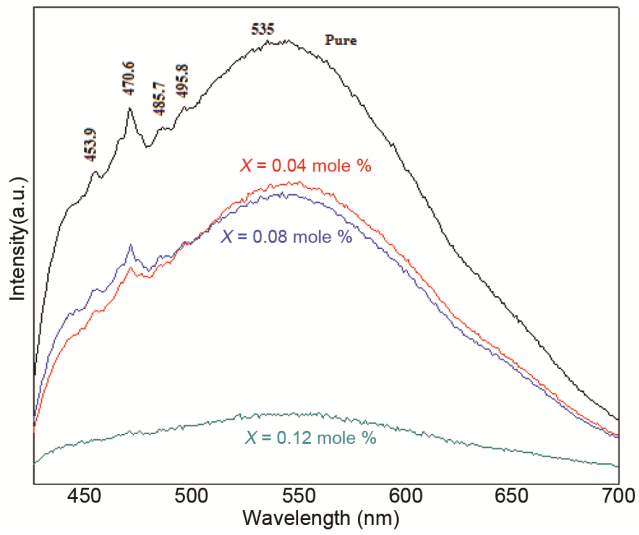

Fig. 6 — Photoluminescence spectra of undoped TiO_2 and co-doped $Ti_{0.95-x}Mo_xN_{0.05}O_2$; x = 0.04, 0.08 & 0.12 mol % nanoparticles.

3.8 Photocatalytic degradation activity

It has been reported that the valence band and conduction band comes from O 2p states and Ti 3d states of TiO_2 respectively[36]. The incorporation of nitrogen into the TiO_2 lattice forms new energy state (N 2p) above the O 2p valence band and Mo doping introduces Mo 4d state below the Ti 3d conduction band which leads to decrease in band gap of TiO_2 and shifts the absorbance in visible region[7,10]. When TiO_2 semiconductor is illuminated by photons of energy equal to or higher than its bandgap energy (Eg), electrons are promoted from the N 2p state to the Mo 4d leading to the generation of electron/hole (e^-/h^+) pairs[4]. These separated electron–hole pair that migrate to the surface are able to initiate oxidation and reduction reactions on TiO_2 Photocatalyst[1]. The reaction mechanism is as described below:

$$TiO_2 + h\nu \rightarrow e^- + h^+ \quad \ldots (3)$$

The photogenerated electrons trapped by Mo^{6+} could transfer to the surface of TiO_2 to react with the oxygen molecules either dissolved in water or present in the atmosphere[10].

$$Mo^{6+} + e^- \rightarrow Mo^{5+} \quad \ldots (4)$$

$$Mo^{5+} + O_2 \rightarrow Mo^{6+} + \bullet O_2^- \quad \ldots (5)$$

These superoxide radical anions react with surface absorbed water molecules to forms $HO_2^\bullet$ which on disproportionation can form hydrogen peroxide.

$$\bullet O_2^- + H^+/H_2O \rightarrow HO_2^\bullet \quad \ldots (6)$$

$$2HO_2^\bullet \rightarrow H_2O_2 + O_2 \quad \ldots (7)$$

Further dimerization of hydrogen peroxide with trapped electrons produces hydroxyl radical (OH•) as given below

$$H_2O_2 + e^- \text{ (trapped)} \rightarrow OH\bullet + H_2O \quad \ldots (8)$$

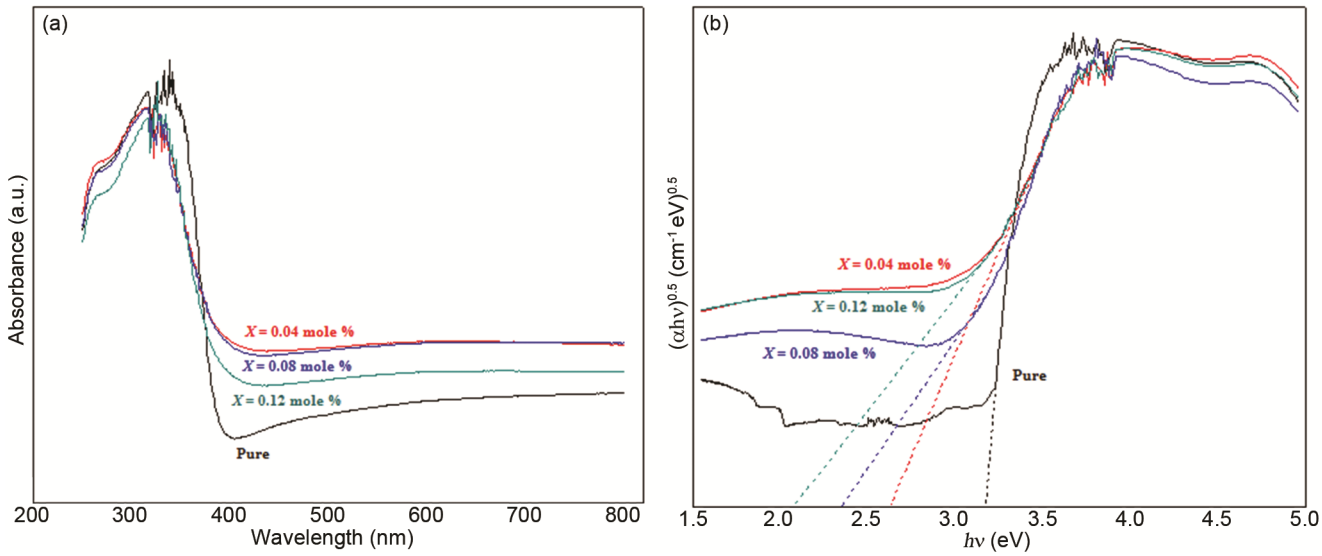

Fig. 7 — (a) UV-Vis. absorption spectra undoped TiO_2 and co-doped $Ti_{0.95-x}Mo_xN_{0.05}O_2$; x = 0.04, 0.08 & 0.12 mol % nanoparticles, (b) Tauc's plot [graph between $(\alpha h\nu)^{1/n}$ *vs* $h\nu$] of undoped TiO_2 and co-doped $Ti_{0.95-x}Mo_xN_{0.05}O_2$; x = 0.04, 0.08 & 0.12 mol % nanoparticles used for determination of energy band gap by drawing an extrapolation of data point represented by dotted line to photon energy axis.

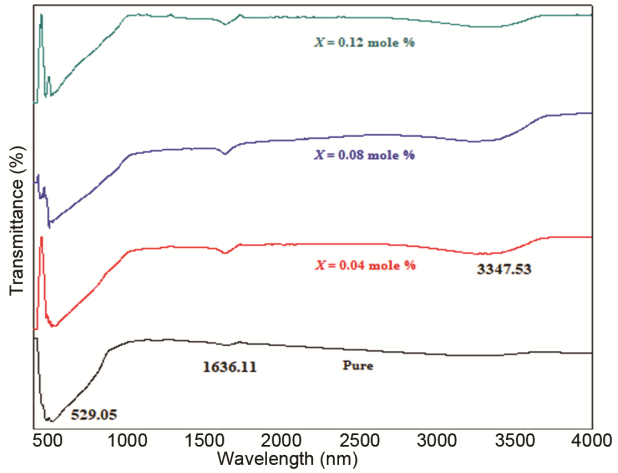

Fig. 8 — FTIR spectra of undoped TiO_2 and co-doped $Ti_{0.95-x}Mo_xN_{0.05}O_2$; x = 0.04, 0.08 & 0.12 mol % nanoparticles.

Moreover, the water molecules and hydroxyl (OH^-) groups adsorbed on the surface of Mo/ N doped TiO_2 could interact with the photogenerated holes from valence band, leading to the formation of strong oxidative species i.e. hydroxyl radicals ($OH^\cdot$)

$$H_2O + h^+ \rightarrow OH\bullet + H^+ \quad \ldots (9)$$

These free radical (OH•) are highly reactive species promote degradation and mineralization of organic pollutants into intermediate compounds as given below

OH• + organic dye (Congo red & methyl orange) → H_2O + CO_2 + intermediate compound (10) Under visible light source illumination the co-doped Photocatalyst dissolved congo red dye solution is completely converted into transparent solution confirm the complete degradation of dye into intermediate compounds i.e. the formation of N-oxides. However in case of methyl orange dye dissolved solution the orange color of dye is slightly change suggest the dye is not degrade in presence of visible light i.e. no formation of intermediate compounds. .

The schematic diagram (Fig. 9) represents reduced band gap after Mo/N co-doping and photocatalytic degradation reaction mechanism under visible light illumination. Photocatalytic activity of the as prepared nanoparticles was tested by using 100 ml solution of 10^{-5} mol/liter concentration of congo red dye containing 0.05 gm of prepared nanoparticles sample. Before the experimental tests, the aqueous suspensions containing photocatalysts was magnetically stirred for 1hr to ensure absorption-desorption equilibrium between the Photocatalyst and CR solution. Then the suspension was irradiated for 120 minutes with phosphorus coated Hg vapour lamp having cutoff filters of wavelength in range (420 nm-520 nm). After regular interval of 20 minutes about 3 ml of solution was sampled, centrifuged (10,000 rpm), filtered and optical absorption was measured by UV-Vis spectrophotometer. The photocatalytic degradation efficiency was determined by following equation:

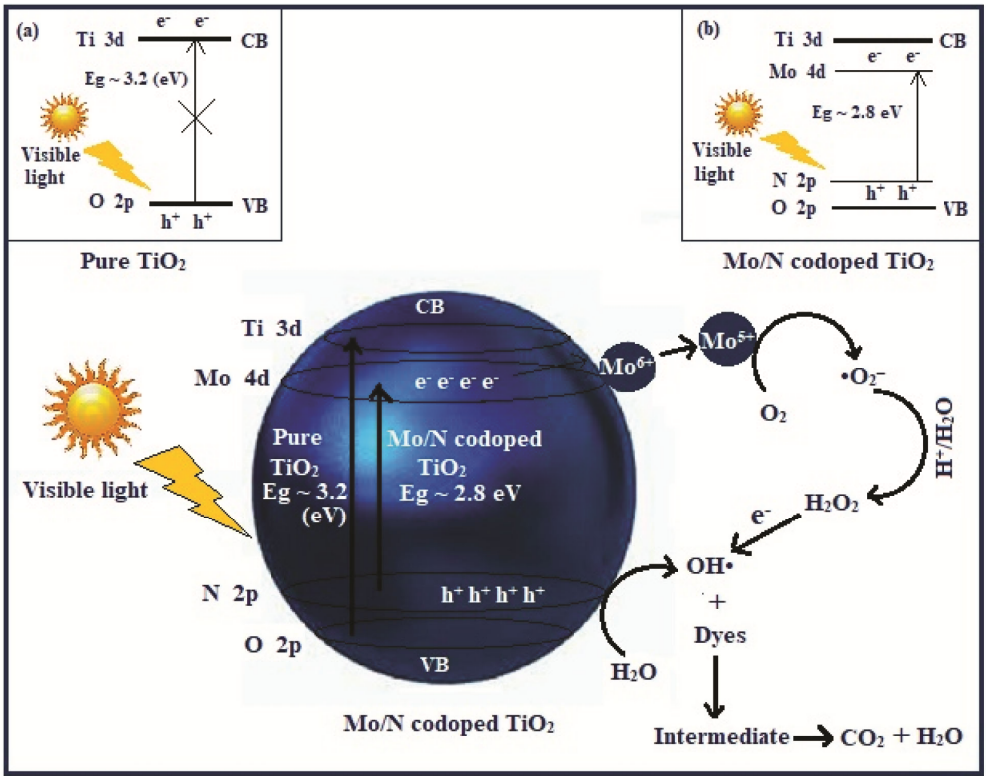

Fig. 9 — The possible mechanism showing photocatalytic degradation of organic dyes by codoped TiO_2 photocatalyst.

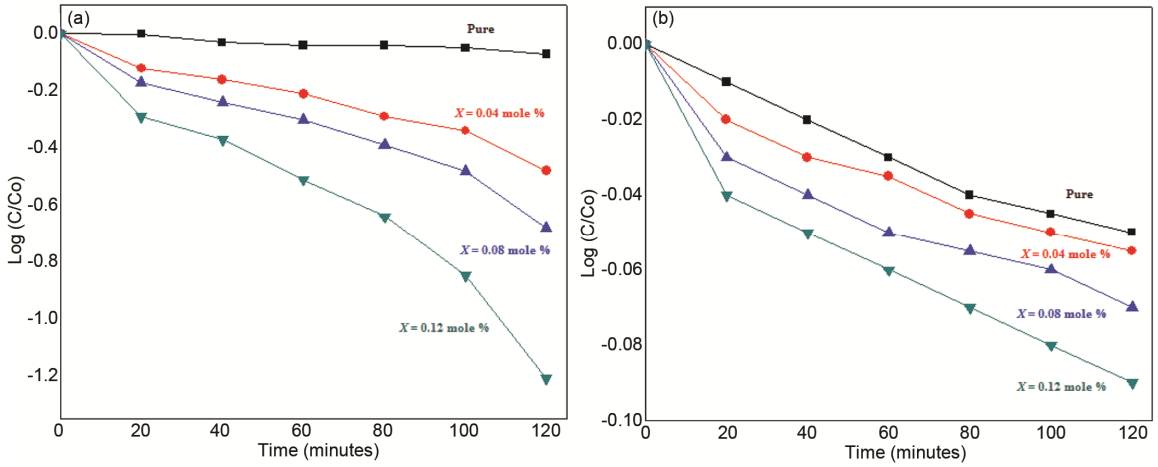

Fig. 10 — (a) Photocatalytic degradation rate of undoped TiO_2 and codoped $Ti_{0.95-x}Mo_xN_{0.05}O_2$; x = 0.04, 0.08 & 0.12 mol % nanoparticles against congo red dye under visible Light, (b) Photocatalytic degradation rate of undoped TiO_2 and codoped $Ti_{0.95-x}Mo_xN_{0.05}O_2$; x = 0.04, 0.08 & 0.12 mol % nanoparticles against methyl orange dye under visible Light.

$$\eta\,(\%) = \frac{(Co - Ct)}{Co} \times 100 \qquad \ldots (11)$$

where C_o is the initial concentration of CR dye solution and C_t is the concentration at particular interval of irradiation time[28]. The photocatalytic degradation efficiency of as-prepared photocatalysts against both dyes is listed in Table 2 and plotted in Fig. 10 (a-b). It is observed that the photocatalytic degradation efficiency of synthesized co-doped nanoparticles for degradation of congo red dye is very high compared to methyl orange dye. On increase in doping concentration degradation efficiency increases and is attributed to decrease in carrier recombination rate and increase in surface area of synthesized Photocatalyst.

Table 2 — Percentage degradation of undoped and co-doped TiO_2 ; $Ti_{(0.95-x)}Mo_xN_{0.05}O_2$; x = 0.04, 0.08 0.12 mol % nanoparticles against Congo red & Methyl orange dyes after exposure to visible light source.

Time (Min)	Congo red				Methyl orange			
	Undoped TiO_2	$(Ti_{(0.95-x)}Mo_xN_{0.05}O_2)$			Undoped TiO_2	$(Ti_{(0.95-x)}Mo_xN_{0.05}O_2)$		
		x = 0.04 mol %	x=0.08% mol %	x=0.12% mol %		x = 0.04 mol %	x=0.08% mol %	x=0.12% mol %
0	0	0	0	0	0	0	0	0
20	0	24	33	49	2	4	7	9
40	6	31	42	57	4	6	8	10
60	8	38	50	69	5	7	10	13
80	9	49	59	77	8	9	12	15
100	11	54	67	86	8	10	13	17
120	14	67	79	94	10	12	15	19

4 Conclusions

Undoped and Mo/N co-doped TiO_2 nanoparticles have been successfully synthesized by sol gel technique. The average particle size of nanoparticles was calculated from the line broadening of (101) peak of XRD pattern and further verified by High Resolution Transmission Electron Microscopy (HRTEM). The decrease in particle size from 28.5 nm to 15.0 nm was observed with increase of Mo concentration. The surface morphology of all samples was studied by Field Emission Scanning Electron Microscopy and shows small agglomeration. The optical band gap energy was found to decrease with increase in doping concentration. The presence of defect levels caused by oxygen vacancies has been confirmed by Photoluminescence spectra. The emission bands observed at 453.9 nm, 470.6 nm, 485.7 nm, 495.8 nm and 535 nm could be arising from the surface sub states appears within forbidden gap of co-doped TiO_2 nanoparticles. The energy dispersive X-ray spectroscopy and Fourier-transform-infrared (FTIR) spectroscopy confirms the formation of stable anatase phase of TiO_2.The Photocatalytic degradation efficiency against congo red dye is very high as compared to methyl orange dye and found to increase with increase in dopant concentration which is attributing to decrease in electron-hole pair recombination rate. On the basis of these observations it is concluded that co-doped TiO_2 nanoparticles are suitable for degradation of congo red dye and are not able to degrade methyl orange dye.

References

1 Qing G, Chuanyao Z, Zhibo M & Xueming Y, *Adv Mater*, 31 (2019) 1901997.

2 Abdul Q K, Shuai Y, Sheng N, Lijuan Z, Wenxue L & Heping Z, *Optics Express*, 25 12 (2017) 539.

3 Hakon E, Said B, Ponniah V, Shivatharsinv Y & Dhavalan V, *Molecules*, 26 (2021) 1687.

4 Khairy M & Zakaria W, *Egypt J Petroleum*, 23 (2014) 419.

5 Karthikeyan C, Parbhakarn A, Ramachandran K, Ali-Mayouf A M, Karuppuchamy S, *J Alloys Compd*, 828 (2020) 154281.

6 Osmín A G, Jaime E V, Rubi R R, Jose L R C, Manuel A A, Dora A S C & Reyna N R, *Catalysts*, 8 (2018) 631.

7 Ansari S A, Khan M M, Ansari M O & Cho M H, *New J Chem*, 40 (2016) 3000.

8 Khan M, Zeng Y, Fawad U, Muhammed N A, Zaman M I & Ullah A, *Mater Res Express*, 4 (2017) 045023.

9 Anna K, Nikolay S, Tatiana K, Anton K, Valery T & Alexander A, *Mater Adv*, 5 (2020).

10 Wang S, Bai L N, Sun H M, Jiang Q & Lian J S, *Powder Technol*, 244 (2013) 9.

11 Haorang D, Guangming Z, Lin T, Changzheng F, Chang Z, Xiaoxiao H & Yan H, *Water Res*, 79 (2015) 128.

12 Seul-Yi L & Soo-Jin P, *J Indus Eng Chem*, 19 (2013) 1761.

13 Matteo C, Alberto V, Elnaz B, David J M, Laura P, Nikolaos D, Ilenia R & Gianguido R, *Catalysts*, 8 (2018) 623.

14 Bing B G, Jie Y, Siyao G, Shen Y & Song H, *Nanoscale Adv*, 2 (2020) 352.

15 Kamaladdin A, Behzad S, Ebrahim M, Kitirote W, Afshin M, Yahya Z, Sonya S & Shadi K, *Mater Res Express*, 9 (2022) 25502.

16 Rani A, Dhiman R L, Singh V, Kumar S & Kumar S, *Nano Express*, 2 (2021) 30002.

17 Mehela K, Barathi D, Ranjith R, Boobas S & Varatharajan K, *J Mater Sci Mater Electron*, 29 (2018) 18111.

18 Sipei Z, Ying X, Wen Z & Peng C, *Mater Chem Phys*, 227 (2022) 125558.

19 Hailin L, Zhihong L, Ling Y, Jing L, Zhanghua G, Chang S, Thing Z, Jing S & Rui X, *Appl Surf Sci*, 257 (2011) 9355.

20 Kumar P M, Kumar E L, Saaikiran A, Govardhan B, Ashok M & Rameshbabu N, *J Alloys Compd*, 825 (2020) 154092.

21 Rani A, Kumar S, Dhiman R L, Singh V & Kumar S, *Indian J Pure Appl Phys*, 60 (2022) 326.

22 Yamanaka K I & Mori K T, *J Phys Chem C*, 116 (2012) 1286.

23 Erdogan N, Xiuwen C, Xiujuan Y & Zipeng X, *J Colloid Interf Sci*, 372 (2012) 1.

24 Park J & Ozturk A, *Ceram Int*, 42 (2016) 16766.

25 Huang J G, Guo X T, Wang B, Li L Y, Zhao M X, Dong L L, Liu X J & Huang Y T, *J Spectroscopy,* 2015 (2015) 681850.

26 Kumaravel V, Rhatigan S, Mathew S, Michel M C, Bartlett J, Nolan M, Steven J H, Gasco A, Ruiz-Palomar C, Daphne H & Pillai S C, *J Phys Mater*, 3 (2020) 025008.

27 Reda S M, Khairy M & Mousa M A, *Arab J Chem*, 13 (2020) 86.
28 Zhang M, Wu J, Hou J & Yang J, *Sci Adv Mater J*, 5 (2013) 535.
29 Cullity B D, Elements of X-ray Diffraction, Reading Mass: Addison–Wesley Publishing Co, (1956) 352.
30 Zhang J, Huang T, Zhang L & Aishui Y, *J Phys Chem C*, 118 (2014) 25300.
31 Komaraiah D, Radha E, Kalarikkal N, Sivakumar J, Ramana Reddy M V & Sayanna R, *Ceram Int*, 45 (2019) 25060.
32 Junbo G, Zhanghua G, Zhihong L, Jing L, Jingjing X, Yang W, Lin L, Hailin L, Jing S, & Rui X, *J Appl Phys*, 114 (2013) 104903.
33 Davis D A, *Japn J Appl Phys*, 32 (1993) 178.
34 Devi L G & Murthy B N, *Catal Lett*, 125 (2008) 320.
35 Parveen P, Viruthagiri G, Mugundan S & Shanmugam N, *Spectrochim Acta Part A: Mol Biomol Spectroscopy*, 117 (2014) 622.
36 Khan M, Junna X, Wenbin C & Liu Z K, *J Nanosci Nanotechnol*, 14 (2014) 6865.